RANS/LIFTING LINE MODEL INTERACTION METHOD FOR THE DESIGN OF DUCTED PROPELLERS AND TIDAL TURBINES

WEIKANG DU
GRADUATE STUDENT, THE UNIVERSITY OF TEXAS AT AUSTIN

SPYROS A. KINNAS
PROFESSOR, THE UNIVERSITY OF TEXAS AT AUSTIN

ROBIN MARTINS MENDES
EXCHANGE STUDENT, ECOLE NAVALE, FRANCE

THOMAS LE QUERE
EXCHANGE STUDENT, ECOLE NAVALE, FRANCE

ABSTRACT

In this paper, a RANS/lifting line model interaction method is proposed to consider the duct geometry in the design of propellers and tidal turbines. In the lifting line model, the Lerbs-Wrench formulas are used for the wake alignment procedure. In the RANS solver, the blade is represented by a pressure jump profile. The blade loading is determined via a previously developed optimization algorithm which takes into consideration the effect of the duct via a simplified image model. An iterative procedure is developed in which the advance ratio (based on the ship speed) and the total thrust in the propeller case and the tip speed ratio (based on the inflow velocity far upstream) are kept constant. The procedure is tested for different cambers and thicknesses of the duct shape for the propeller case and different duct angles for the turbine case. The efficiency, inflow velocity and thrust on the blade and duct are obtained and analyzed. In the propeller case, the influence of different factors, including the blade number, drag-to-lift ratio, advance ratio and thrust coefficient, are studied. This method is proved to be reliable and efficient in designing ducted propellers and tidal turbines.

Keywords: ducted tidal turbines and propellers, optimization, lifting line method, Reynolds Averaged Navier-Stokes (RANS) method, Lerbs-Wrench formulas

INTRODUCTION

The lifting line model is widely used in the first step of propeller and tidal turbine design to obtain the optimal loading on the blades in given conditions, and the results are then used in more accurate methods like the boundary element method (BEM) (Lee, 1987) and the vortex lattice method (VLM) (Kerwin et al. 1978). Xu (2010), Kinnas et al. (2012) and Menéndez (2013) followed this designing procedure and used a non-linear optimization code (CAVOPT-3D) and a data-base searching code (CAVOPT-BASE) to design the geometry of the propeller blades and tidal turbine blades, and compared the results with those from RANS solver. In the lifting line model, a simple way to consider the influence of the wake is by assuming a constant trailing pitch angle along the x-direction, known as the Betz condition (Kerwin et al., 2010). The induced velocities (both axial and tangential) can be evaluated by the formulas proposed by Lerbs et al. (1952) and Wrench et al. (1957). Menéndez et al. (2014) used an improved fully aligned wake model and had an assessment of the Betz condition.

In the lifting line model, the key blade is presented by discretized horseshoe vortices (Kerwin et al., 2010). The effect of the hub and duct can be considered by placing image vortexes for every vortex located on the blade. However, the image model for the duct is equivalent to the assumption that the length of the duct is infinite and the blade is placed in an infinite cylindrical tunnel. The shape of the duct is neglected, so this method is neither accurate nor plausible in the designing of the duct geometry.

In this paper, a Reynolds-Averaged Navier-Stokes (RANS)/lifting line model interaction method is proposed to consider the duct geometry in the design of ducted propellers and tidal turbines, and a numerical code called LLOPT2NS (lifting line optimization to Navier-Stokes) is developed. In this method, the Lerbs-Wrench formulas are used in the wake alignment procedure. In the propeller case, the duct is built by using a NACA a=0.8 camber line and a NACA 00 thickness distribution with the angle of attack fixed as 10 degree. The influence of the maximum camber and thickness on the efficiency, inflow velocity, KT and 10KQ are studied. Different factors on the results, including the advance ratio, the drag-to-lift coefficient, the number of blade, and the tip speed ratio, are compared with those obtained by running the propellers without ducts or by using the image model for the duct in the lifting line method without considering the real geometry. In the turbine case, the duct is rotated by different angles, and the effect on the efficiency is studied. Results show that the properly-designed duct can increase the efficiency of both propellers and tidal turbines significantly. The blade optimized loading can be used in designing the blade geometry and by using the VLM/RANS coupling method (Kinnas et al., 2013) or the BEM/RANS coupling method (Kinnas et al., 2016) on the ducted propeller and tidal turbines, this results from this paper can be tested.

METHODOLOGY

The actuator disk model

(a) **Propeller case**   (b) **Turbine case**
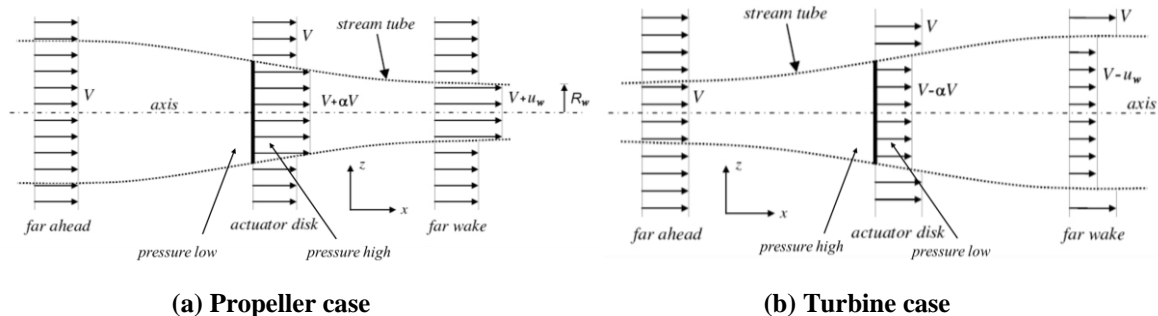
Figure 1 Inflow velocity and pressure change in the actuator model

In the actuator disk model (Menéndez, 2013), the propeller and turbine blades are represented by a surface called an actuator disk. As shown in Figure 1, in the propeller case, the flow velocity increases because of the energy from the ship machinery, and from Bernoulli's equation the pressure decreases. There is a pressure jump on both sides of

the actuator disk, and the low-pressure side is the left-hand side of the actuator disk for the inflow in the given direction. The integration of the pressure differences on both sides is the thrust acting on the propeller blade. In the turbine case, the velocity decreases and the low-pressure side is the right-hand side of the actuator disk.

The lifting line model with Lerbs-Wrench formulas

In the lifting line mode, the propeller and turbine blades are represented by M discretized horseshoe vortices, as shown in Figure 2 (Menéndez, 2013). The Lerbs-Wrench formula is given in Equation (1) which determines the shape of the wake.
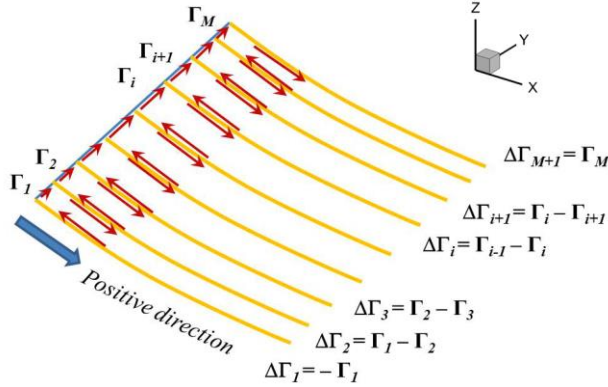
Figure 2 The lifting line model and the line vortex   **Figure 3 The image model for the hub**
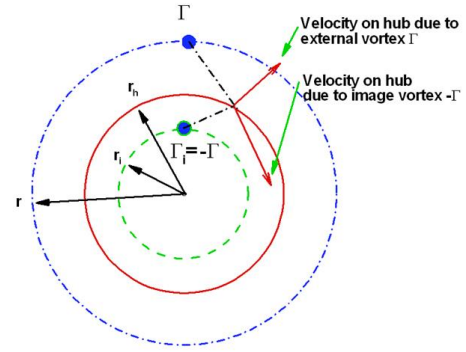
$$\frac{\tan(\beta)}{\tan(\beta_i)} = \gamma\sqrt{1 - w_x(r)} \qquad (1)$$

where β is the undisturbed wake pitch angle, β_i is the wake pitch angle, $w_x(r)$ is the axial wake fraction distribution and γ is a constant.

The image model for the hub and duct

In the lifting line model, the influence of the hub and duct can be considered by in an image model, as shown in Figure 3 for the hub case. For each vortex located at radius r_v, an image vortex with the same strength but different sign is located at radius r_{image}, which is given in Equation (2). The length of the duct in the image model is infinite, so the blade is place in an infinite cylindrical tunnel. It should be noted that in this paper, the images of the image (when there are both a hub and a duct) are not considered.

$$r_{image} = \frac{r_h^2}{r_v} \qquad (2)$$

where r_h is the hub radius.

The RANS/lifting line model interaction method

In this paper, an iterative method is proposed to couple the RANS method for the duct with the lifting line method for the propellers and tidal turbines. In the propeller case, the far upstream inflow velocity is V_s (ship speed). The advance ratio J_s and the propeller rotational frequency *n* are kept constant through the iterations. The advance ratio J_s is defined in Equation (3) and the local advance ratio is defined in Equation (4).

$$J_s = \frac{V_s}{nD} \qquad (3)$$

where the subscript *s* means *ship*, *D* is the diameter of the propeller and n is the rotational frequency.

$$J_l = \frac{U_{in}}{nD} \qquad (4)$$

where the subscript *l* means *local*, and U_{in} is the inflow for the lifting line model. U_{in} is different from the ship speed because the inflow velocity is influenced by the duct, as shown in Figure 1.

The total thrust coefficient C_{Ts} is nondimensionalized by the ship speed as in Equation (5).

$$C_{Ts} = \frac{T_T}{\frac{1}{2}\rho\pi V_S^2 R^2} \tag{5}$$

where R is the radius of the propeller blade, and T_T is the total thrust.

The total thrust can be divided into two parts: the propeller-provided thrust T_P and the duct-provided thrust T_D. A nondimensionalized factor τ is defined as

$$\tau = \frac{T_P}{T_P + T_D} = \frac{T_P}{T_T} \tag{6}$$

where $\tau > 1$ means there is drag on the duct and $\tau < 1$ means the duct provides extra thrust.

The local thrust coefficient and the torque coefficient from the lifting line model is defined in Equation (7) and (8). The efficiency of the propeller is defined in Equation (9).

$$C_{Tl} = \frac{T_P}{\frac{1}{2}\rho\pi U_{in}^2 R^2} = \tau C_{Ts}\frac{V_S^2}{U_{in}^2} \tag{7}$$

$$C_Q = \frac{Q}{\frac{1}{2}\rho\pi V_S^2 R^3} \tag{8}$$

$$\eta = \frac{T_T V_S}{Q\omega} \tag{9}$$

where $\omega = 2n\pi$ is the propeller angular velocity.

Plug Equation (3~8) into Equation (9), the final expression for the propeller efficiency is shown in Equation (10).

$$\eta = \frac{J_s C_{Ts}}{\pi C_Q} \tag{10}$$

where J_s and C_{Ts} are both constant and the only changing variable during the iterations to in the efficiency equation is the torque coefficient C_Q.

In the RANS/lifting line model interaction method, the flow around the duct is solved in the RANS solver, and the inflow velocity for the lifting line model is modified considering the influence of the duct. The code for the lifting line model is called LLOPT (Lifting Line OPTimization). It should be noted that the swirl component of the induced velocity is not included in the RANS model, assuming that it will not affect the thrust (which is in the axial direction) and the inflow upstream. A flow chart of the coupling process is shown in Figure 4.

The viscous effect in the RANS/lifting line model interaction method is considered in two parts: the viscosity on the duct is considered as a non-slip boundary condition in the RANS model, and in the lifting line model a drag-to-lift ratio is use, as shown in Equation (11).

$$\kappa = \frac{C_D}{C_L} \tag{11}$$

where C_D is the sectional drag coefficient and C_L is the sectional lift coefficient.

In the RANS model, the actuator disk is represented as a *fan* boundary condition with a pressure jump profile as a function of the sectional radius r, calculated in Equation (12) and (13).

$$\Delta T = \rho Z\Gamma[(\omega r + u_t^*) - \kappa(U_{in} + u_a^*)]\Delta r \tag{12}$$

where Z is the number of blades.

$$\Delta p = \frac{\Delta T}{2\pi r \Delta r} \tag{13}$$

where u_t^* and u_a^* are the tangential and axial inducted velocities, respectively, and Γ is the optimized circulation on the blade, calculated from the lifting line model.

In the propeller case, the inflow velocity for the lifting line model is calculated by using Equation (14).

$$U_{in} = U_{RANS} - u_a^* \tag{14}$$

where U_{RANS} is the averaged velocity at the actuator disk from the RANS solver, and u_a^* is the averaged axial induced velocity from the previous iteration, calculated from the lifting line model.
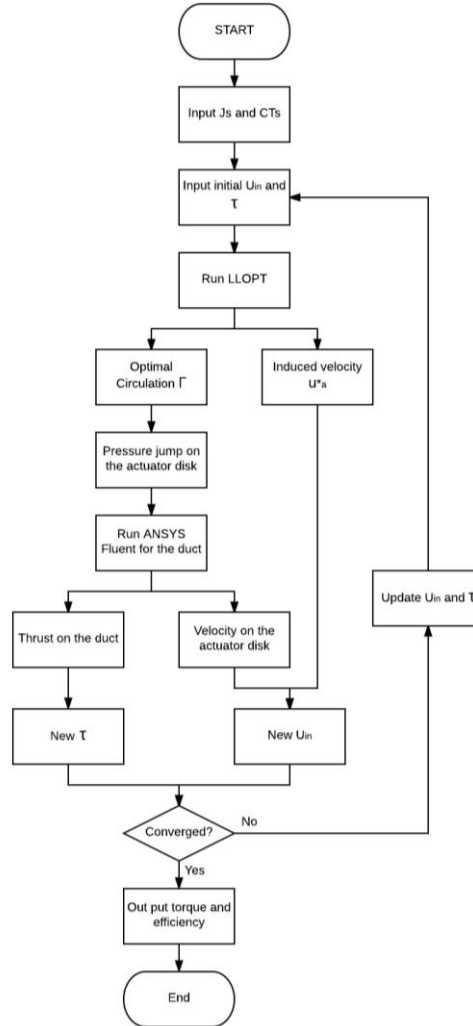
Figure 4 Flow chart of the RANS/lifting line model interaction method (propeller case)

In the tidal turbine case, the coupling scheme is the similar with the propeller case except the following details. First, in this case the thrust is not of interest so only the inflow velocity is evaluated and updated during the iterations. Second, there is no advance ratio and thrust coefficient in this case. Instead, the far upstream tip speed ratio (TSR) is kept constant. Third, the inflow velocity is calculated in Equation (15) because the inflow decelerates as it approaches the actuator disk, as shown in Figure 1.

$$U_{in} = U_{RANS} + u_a^* \tag{15}$$

In the turbine case, the efficient is defined as the useful power from the blade over the total energy in this area, as shown in Equation (16).

$$\eta = \frac{Q\omega}{\frac{1}{2}\pi\rho V_S^3 R^2} \tag{16}$$

where R is the radius of the turbine blade, consistent with the propeller case.

RESULTS AND DISCUSSION

The following runs for the propeller case have been performed in this paper:
- **Propeller_case1**: lifting line method for open propeller (no hub), without coupling with RANS (only the code LLOPT is used);
- **Propeller_case2**: lifting line method for propeller (no hub) inside a cylindrical tunnel, without coupling with RANS (only the code LLOPT is used);
- **Propeller_case3**: the RANS/lifting line model interaction method for propeller with real duct geometry (no hub) coupled with RANS (the code LLOPT2NS is used).

It should be noted that the current model can run a ducted propeller without a hub, but has not been reliable when a hub is included, so all the propeller cases in this paper are performed without a hub.

The following runs for the tidal turbine case have been performed in this paper:
- **Turbine_case1**: lifting line method for open turbine (with hub), without coupling with RANS (only the code LLOPT is used);
- **Turbine_case2**: the RANS/lifting line model interaction method for turbine with real duct geometry (with hub), coupled with RANS (the code LLOPT2NS is used).

1. The image model
The effects of the image from the lifting line model are shown in Figure 5. If there is no duct or hub, the circulation goes to zero at both the tip and the hub. With the image model, the gradient of the circulation goes to zero near the image, and the circulation profile is "flat". The full cosine spacing is applied for the case without hub or duct case, since it concentrates more panels near the blade tip and root, where the gradient of the circulation is big. The half cosine spacing is applied when only one side of the image model is used, and less panels are used where the gradient for the circulation profile is small. The total number of panels is 70 for both cases. More discussion about the spacing and the panel numbers can be found in the appendix.
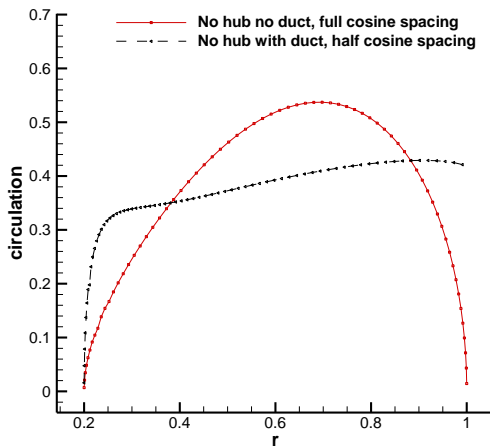
Figure 5 Effect of the image on the circulation (propeller case)
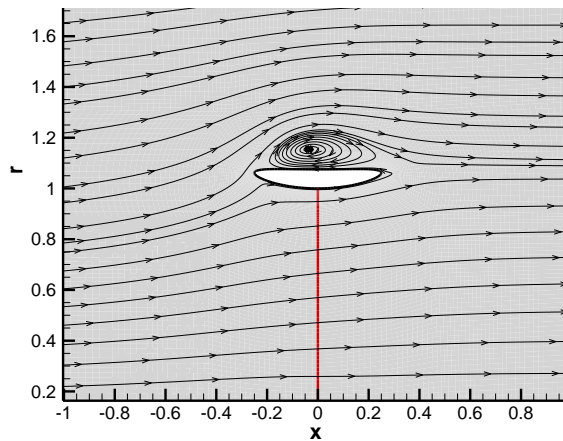
Figure 6 Flow field for duct with symmetry geometry (turbine case)

2. The Axisymmetric RANS model

Originally, to enable the tidal turbine to work with flow in both directions, the duct was designed by using parabolic camber distribution and elliptic thickness distribution, as show in Figure 6. However, since the inflow is decelerating as it approaches the actuator disk, reverse flow is likely to happen, which is apparently not normal. To avoid this problem, the idea of using symmetry geometry is abandoned, and the duct is built by super-imposing a NACA a=0.8 camber and a NACA00 thickness, the same as the propeller case. The duct is rotated around the blade tip by certain angles, and is placed along the streamline shown in Figure 1. The length of the duct in the propeller case is 1 (nondimensionalized by the blade radius) and in the turbine case is 0.5. The influence of the duct length in the interaction method will be studied in the future.

The domain and mesh of the duct in the RANS model are shown in Figure 7. In the propeller case, the geometries shown in the figure as samples are the cases where the camber equals -0.03 and the thickness equals 0.2. In the turbine case, the camber equals -0.05 and the thickness equals 0.15. Negative camber makes more flow go into the actuator disk plane and thus improve the performance of propellers and turbines. In the propeller case, the duct angle, which is defined by the baseline of the duct and the axial direction, is kept constant as -10 degrees (with counter clock wise being positive). In the turbine case, this angle is an variable and influence on the efficiency will be studied.

In both cases, the total grid number is about 50k. To make sure that the first layer of the mesh does not fall into the buffer layer, the y plus on the duct for the propeller case is over 50 and for the turbine case is over 40. The $k - \omega$ with SST turbulence model is used in the RANS solver and the Reynolds number is 10^6.

(a) Propeller case   (b) Turbine case
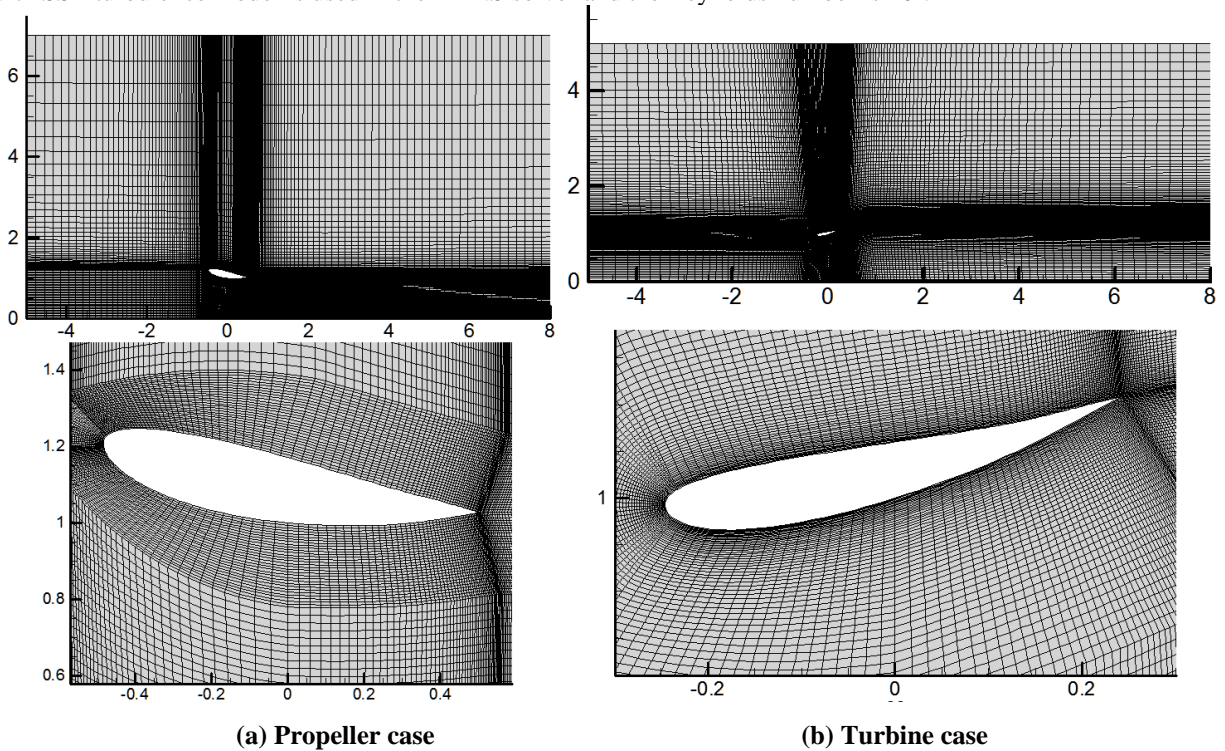
Figure 7 Sample mesh in the RANS model

The pressure contour plots are shown in Figure 8. There is a discontinuity at the actuator disk because a pressure jump profile is used in the fan boundary condition. The high-pressure side and low-pressure side are consistent with Figure 1.

(a) Propeller case   (b) Turbine case
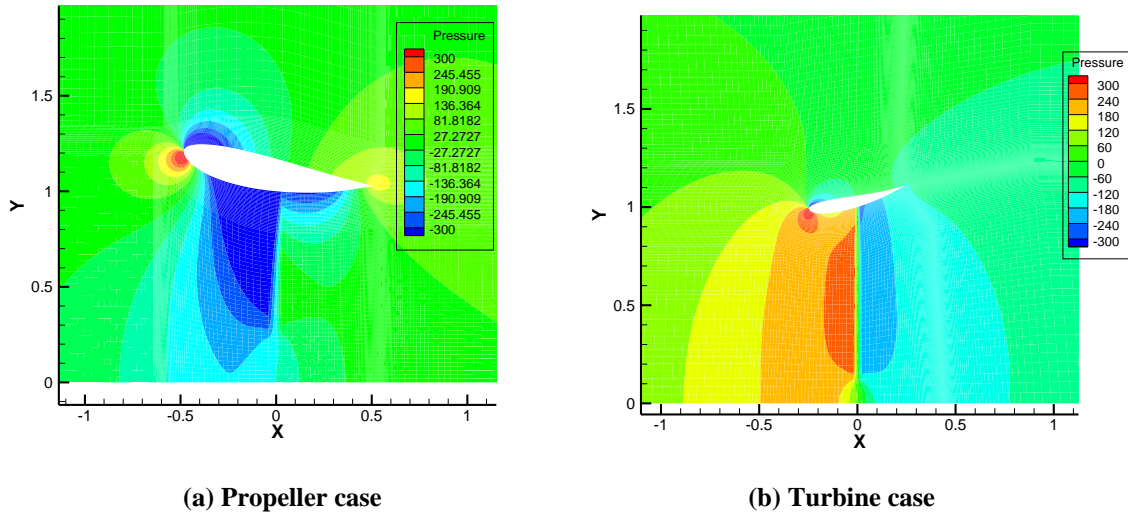
Figure 8 Pressure contour in the RANS model, pressure jump is shown by the discontinuity at the actuator disk (Plotted with U_{in}=1m/s, $\rho = 1000 kg/m^3$ and the reference location is at the far upstream)

3.1. Propeller case, J_s=0.5, C_{Ts}=1.0, influence of the duct geometry

In this case, the advance ratio and total thrust coefficient defined by the velocity at far upstream are fixed and different duct geometries are used in the RANS/lifting line model interaction method. For the camber, three maximum camber f_0 are used, including -0.02, -0.03 and -0.04. For each f_0, four maximum thickness t_0 are selected, including 0.15, 0.20, 0.25 and 0.30, so there are 12 different duct geometries in total. In each geometry, the duct is located from -0.5 to 0.5 in the x-direction, and in the r-direction, the middle point of the lower side is always at location (0,1), because the radius of the blade is 1. Each geometry is rotated by 10 degree in the clock-wise direction around point (0,1), giving a 10-degree angle of attack for the inflow coming from left to the right along x-direction. The four most "extreme" geometries are shown in Figure 9.
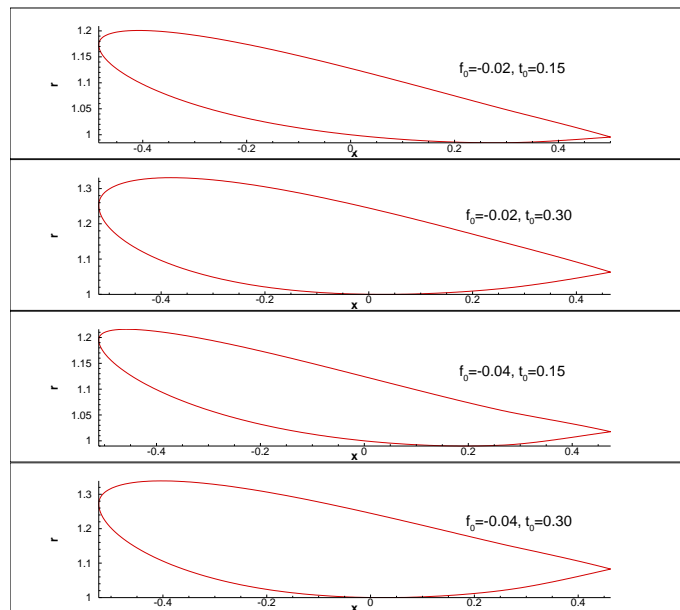
Figure 9 The most "extreme" duct geometries for the propeller case

Table 1 Input for LLOPT in the propeller case

Hub radius	0.2
Number of blades	3
Number of panels	70
κ	0.05
Image model	Duct only
Spacing	Half cosine with more panels near hub

Other parameters for the lifting line model is listed in Table 1 and used as input for LLOPT. The spacing is consistent with the image model. In the code LLOPT2NS, the tolerance for U_{in} and τ are 0.001, and each case converges within several iterations. For the case $f_0 = -0.03$ and $t_0 = 0.2$, the convergence history for the pressure jump and circulation on the blade are shown in Figure 10, and the convergence history for U_{in} and τ are shown in Figure 11. From those figures, it is shown that the solutions from the first iteration to the second iteration change most comparing with other iterations.
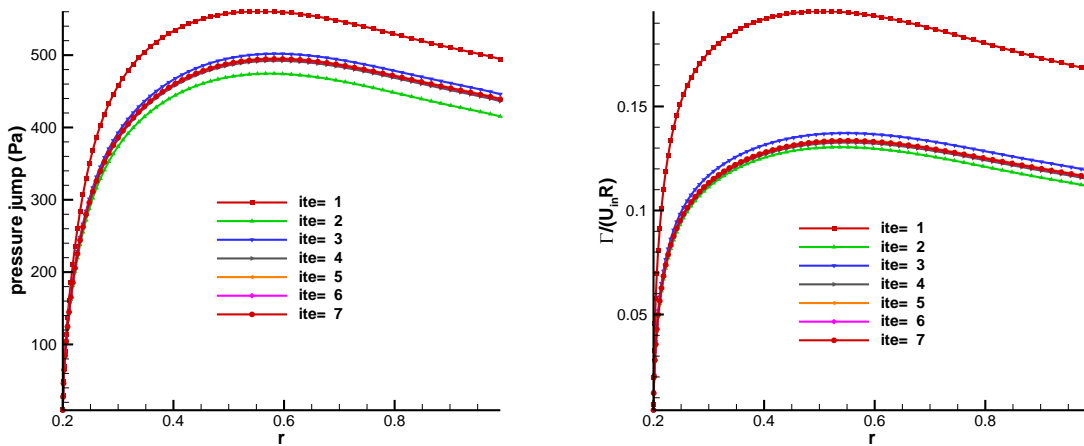
Figure 10 The convergence history of pressure jump and circulation
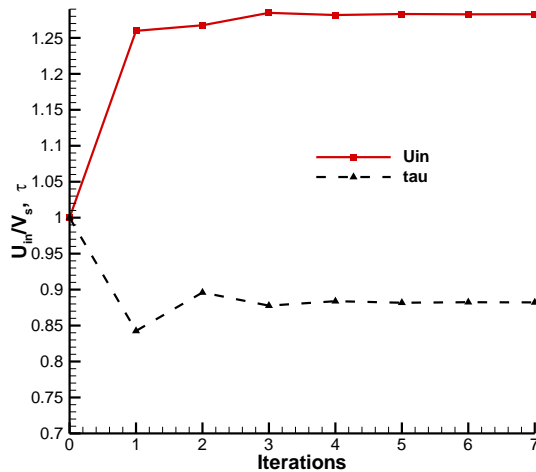
Figure 11 The convergence history of U_{in} (mean inflow) and τ

In Propeller_case3, the efficiencies of different duct geometries are shown in Figure 12, together with the efficiencies from Propeller_case1 and Propeller_case2 for the same advance ratio and thrust coefficient. The KT and 10KQ are plotted in Figure 13 and the inflow velocity and τ are shown in Figure 14. If the duct has bigger camber or thickness, the mean inflow for the actuator disk will be higher, and more thrust will be generated by the duct, so τ is smaller. If the duct geometry is not considered, all the thrust will be generated from the propeller blade, so for given total thrust, the KT will the same for Propeller_case1 and Propeller_case2, as shown in Figure 13. In Figure 14, the thrust contributed from the duct may vary from less than 5% to more than 20%, depending on different duct geometries for the given J_s and C_{Ts}. It is shown that the increase of camber of the duct can increase the efficiencies. If the duct geometry is not considered (Propeller_case2), the efficiency will be overestimated, so without coupling with RANS for the real duct geometry, the results are not accurate. It is also shown that in the given J_s and C_{Ts}, the duct can increase the propeller efficiency. For higher thrust, the benefit from the duct in the efficiency is even higher, as shown in Figure 15.
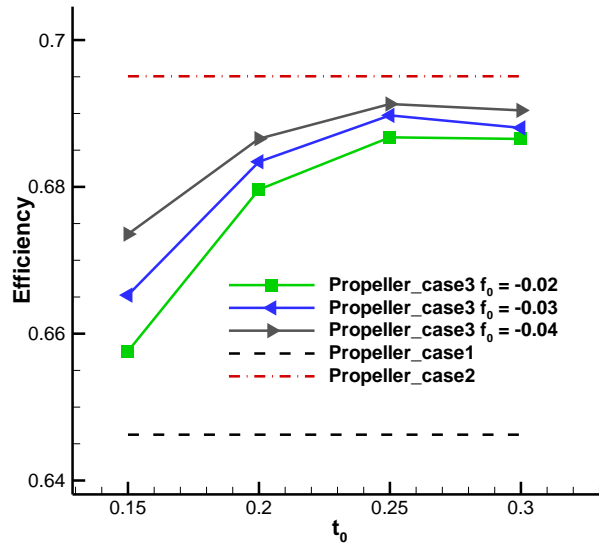
Figure 12 Efficiency for the propeller case for various duct geometries (J_s=0.5, C_{Ts}=1.0)
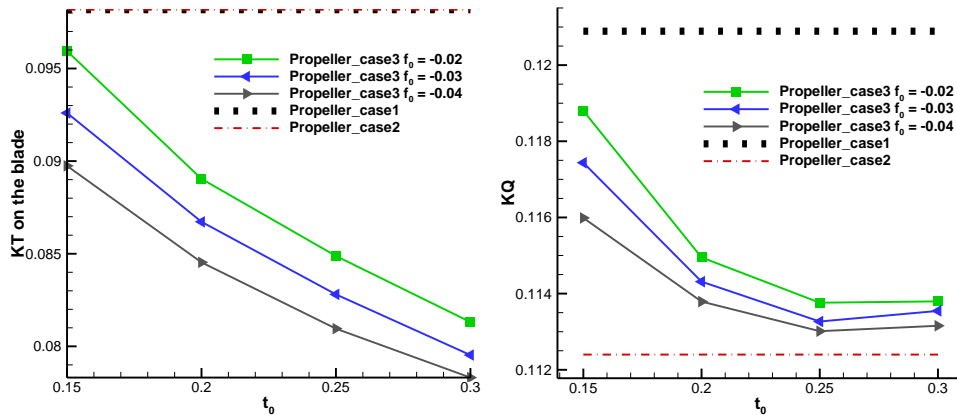
Figure 13 The KT and 10KQ on the blade for the propeller case for various duct geometries (J_s=0.5, C_{Ts}=1.0)
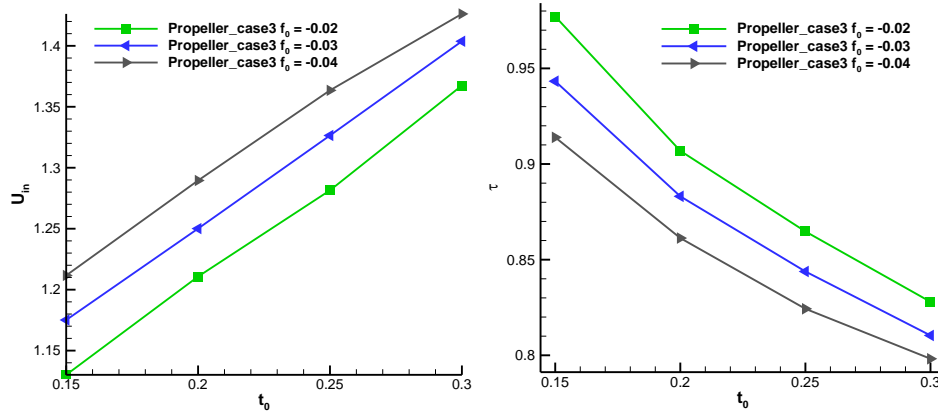
Figure 14 The inflow velocity and τ for the propeller case for various duct geometries (J$_s$=0.5, C$_{Ts}$=1.0)

(a) C$_{Ts}$=2.0   (b) C$_{Ts}$=3.0
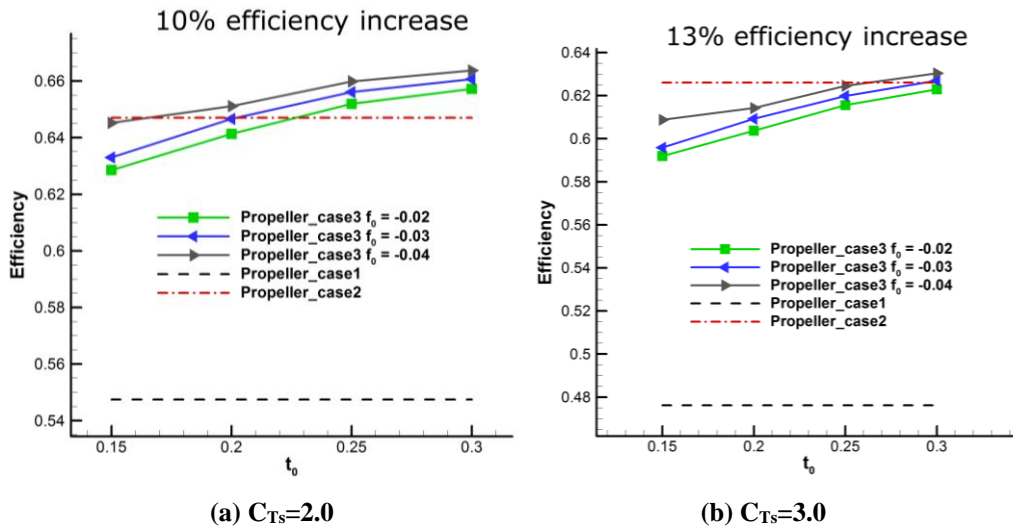
Figure 15 Efficiency for the propeller case for various duct geometries with higher C$_{Ts}$ (J$_s$=0.5)

However, based on the following three reasons, the conclusion in this part must be evaluated more carefully and proper tests are needed in the future. First, in this paper the Lerbs-Wrench formulas are used for the wake alignment procedure, which is suitable in this iterative method due to its high computational efficiency, but may not be as reliable as the more complicated full wake alignment model. By using full wake alignment, the results of both the propeller case and the turbine case might change. Second, the swirl component of the induced velocity is not considered in the RANS model, assuming that neglecting the swirl will not influence the thrust on the duct and the axial velocity in the inflow. This assumption needs to be better justified and the torque might be represented by the body force in the tangential direction, which will be addressed in future work. Third, as shown in Figure 14, the mean inflow velocity for some duct geometries can be 40% higher than the velocity at far-upstream, which might cause cavitation or separation and the high efficiency might not be achieved. The efficiency needs to be further verified after the blade geometry is designed based on the circulation, and then tested with other numerical tools, like by coupling of BEM or VLM method with the RANS solver. More details about these methods can be found in Kinnas et al. (2013) and Kinnas et al. (2016).

3.2. Propeller case, f_0 = -0.03 and t_0 = 0.2, influence of J_s and C_{Ts}

In this case, the duct geometry is fixed with f_0 = -0.03 and t_0 = 0.2. The duct shape is shown in Figure 7. In Figure 16(a), the advance ratio changes from 0.5 to 1.0 for given C$_{Ts}$ as 1.0, and in Figure 16(b) the total thrust coefficient is selected among 1.0, 1.5, 2.0, 2.5 and 3.0 for given J$_s$ as 0.5. Other parameters are the same as in Table 1. For a fixed

thrust, with the increase of advance ratio, the efficiency decreases in Propeller_case1 while increases in Propeller_case2, and the difference in efficiency between Propeller_case1 and Propeller_case3 increases. It should also be noted that as J_s is higher, the error from the image model becomes higher compared with the case with a real duct geometry.

For a fixed advance ratio, with the increase of thrust, the efficiency decreases in all three cases. The difference in efficiency between Propeller_case1 and Propeller_case3 increases. In other words, the benefit by using a duct increases with the increase of advanced ratio and the thrust coefficients.

| (a) Fixed C_{Ts} as 1.0 | (b) Fixed J_s as 0.5 |
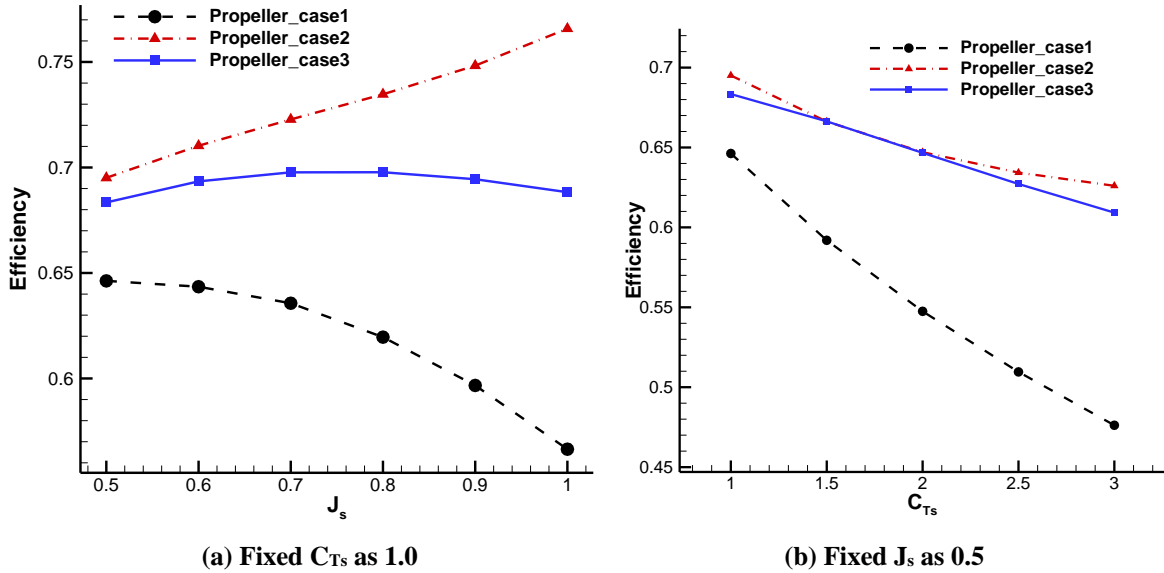
Figure 16 The efficiencies for a fixed duct geometry with changing J_s and C_{Ts}

The inflow velocity and τ are shown in Figure 17. U_{in} and τ are not as sensitive to the change of advance ratio as to the thrust, and for high thrust, the inflow velocity can be increased by over 60%.

| (a) Fixed C_{Ts} as 1.0 | (b) Fixed J_s as 0.5 |
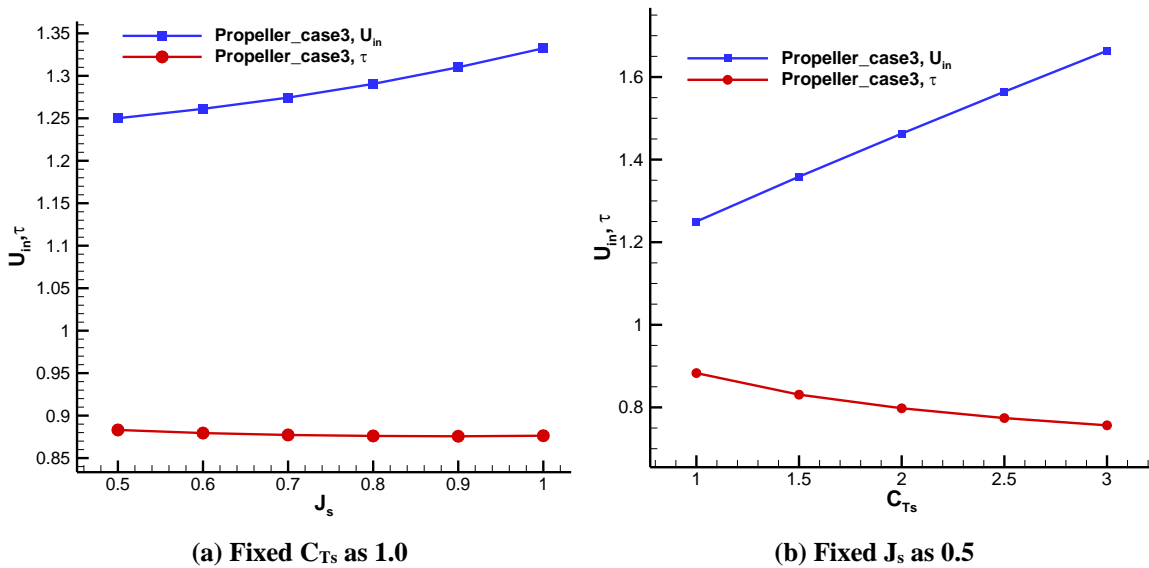
Figure 17 The inflow velocity and τ for a fixed duct geometry with changing J_s and C_{Ts}

3.3. Propeller case, influence of the blade number

In all the above cases, the number of blade is kept constant as 3. The influence of the blade number is studied in this section and results are shown in Figure 18. In Propeller_case3, the duct geometry is f_0 = -0.03 and t_0 = 0.2, as shown in Figure 7. The advance ratio is 0.5 and thrust coefficient is 1.0, and other parameters are the same as in Table 1.
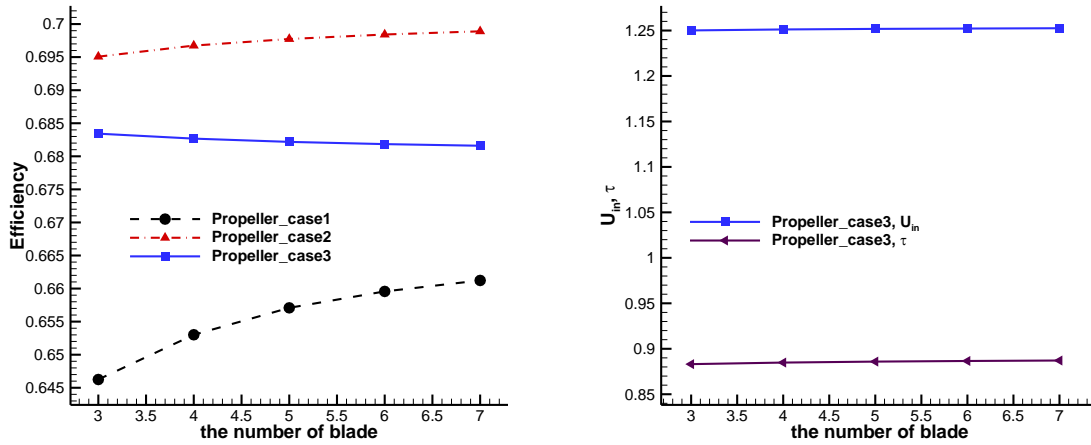
Figure 18 The influence of blade number, fixed duct shape, J_s and C_{Ts}

As shown in the figures above, as the blade number increases, the efficiencies from Propeller_case1 and Propeller_case2 both increase, but in Propeller_case3, the efficiency decreases slightly and the inflow and thrust on the duct are almost constant.

3.4. Propeller case, influence of κ

In the lifting line model, the viscous effect on the blade is taken into consideration by adding a drag-to-lift ratio κ. In the above sections κ is kept constant as 0.05. In this section, κ varies from 0 (without any viscous effect on blade) to 0.05. The duct geometry is f_0 = -0.03 and t_0 = 0.2, as shown in Figure 7. The advance ratio is 0.5 and thrust coefficient is 1.0, and all the other parameters are the same as in Table 1.
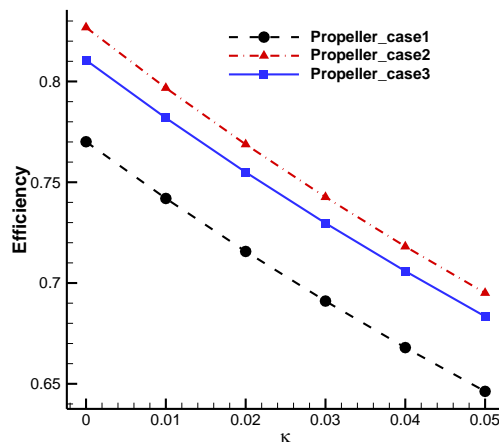
Figure 19 The influence of drag-to-lift ratio on the efficiency, fixed duct shape, J_s and C_{Ts}

As shown in Figure 19, as the drag-to-lift ratio increases, the efficiency decreases because more energy is consumed by friction. It is also shown that without consider the real duct geometry, the image model over-predict the efficiency.

4. Turbine case, influence of the duct angle

In this case, the length of the duct is kept constant as half of the blade radius. The duct geometry is produced by super-imposing a NACA $a = 0.8$ camber with $f_0 = -0.05$ and a NACA 00 thickness with $t_0 = 0.15$, and rotated around the blade tip (0,1) by different angles, as shown in Figure 20. Other parameters in the lifting line model is shown in Table 2.

Table 2 Input for LLOPT in the turbine case

Hub radius	0.2
Number of blades	3
Number of panels	70
κ	0.05
Image model	Hub and duct
Spacing	Constant
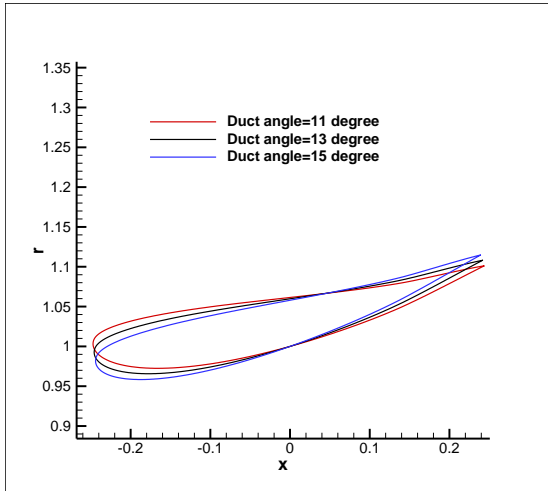
Figure 20 Different duct shapes tested
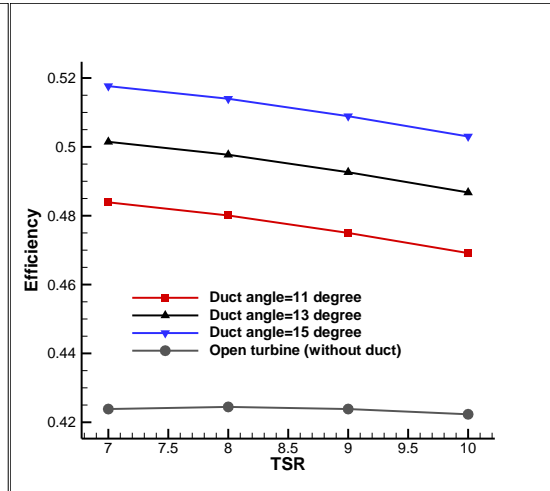
Figure 21 The efficiency increase after implementing a duct in the current turbine

Compared with the open turbine, the efficiency increase due to the presence of duct can be in the range of 11% to 22%, as shown in Figure 21. The benefit of the duct is obvious. It is also found that as the duct angle is increase, the efficiency will be higher. The optimal duct angle for given design conditions will be studied in the future.

The convergence history for the pressure jump and velocity inflow are similar with that of the propeller case, so it is not shown here. It should be noted that in the RANS/lifting line model interaction method for the turbine case only the velocity inflow is updated during each iteration, and the pressure jump is negative, as shown in Figure 8.
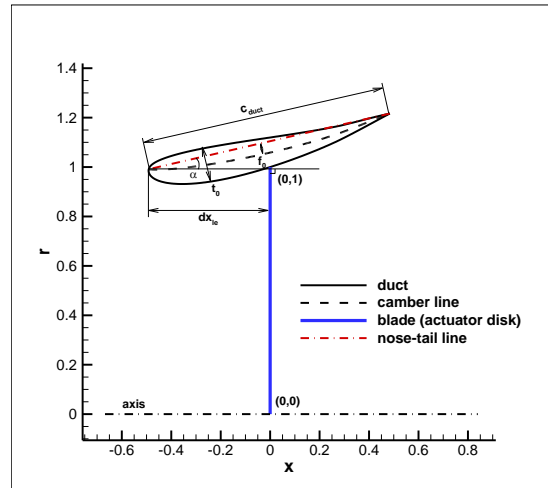
Figure 22 Parameters to determine the duct geometry (f_0, t_0, duct angle α, chord length c_{duct}, duct location dx_{le}, etc.)

In this paper, the only parameter that is changed in the turbine case is the duct angle. However, with the interaction method proposed in this paper, the duct can be designed in a more complete way. A few parameters to control the geometry of the duct are shown in Figure 22. Influence of those parameters on the design of the ducts and the efficiencies will be studied in detail in the future.

CONCLUSIONS AND FUTURE WORK

In this paper, a RANS/lifting line model interaction method is proposed for the design of ducted propellers and tidal turbines, and a numerical code called LLOPT2NS is developed and tested for different cases. Results show that this method is efficient and reliable. In the lifting line model, a simplified image model can be used to consider the effect of the hub and the duct, and the appropriate spacing is adopted. Lerbs-Wrench formulas are used for the wake alignment procedure. In the RANS model, flow around the duct with real geometry is solved and results are coupled with the lifting line model in an iterative way. The viscous effect is considered by adopting a drag-to-lift ratio in the lifting line model and by the non-slip wall boundary condition in the RANS model. The duct is built with a NACA a=0.8 camber and a NACA 00 thickness distribution. In the propeller case, the duct angle is fixed as 10 degree and the influences of the camber and thickness on the efficiency are studied. In the tidal turbine case, the influence of the duct angle is studied. In both cases the camber is negative so the duct can bring flow into the actuator disk.

In the lifting line model, by comparing the efficiencies with the open case and the duct case with image model, it is shown that the duct can increase the efficiency, but without coupling with the RANS method, the duct geometry is not considered.

In the RANS/lifting line model interaction method, with the increase of camber and thickness, the efficiency, local inflow velocity and thrust on the duct all increase while the KT and KQ on the blade decrease for the propeller case. For fixed duct geometry, it is shown that the efficiency and local inflow velocity increase with the increase of advance ratio and total thrust coefficients. As the blade number and drag-to-lift number increase, the efficiency for the ducted propeller decreases.

In the turbine case, the efficiency will increase as the increase of duct angle for fixed camber and thickness distribution. The benefit can be as high as over 20%. Different parameters that determines the duct geometry are presented for designing the duct.

In the future, the effect of those parameters will be studied for both the propeller case and the turbine case. Fully aligned wake alignment model will be used to replace the Lerbs-Wrench formula. The swirl component of the induced velocity will be added in the RANS model as body forces in the tangential direction. Furthermore, the blade geometry

will be designed based on the optimal circulation from this method, and analyzed by coupling the panel method or the vortex lattice method with the RANS solver to see if the circulation can be recovered.

ACKNOWLEDGEMENTS

REFERENCES

Kerwin, Justin E., and Jacques B. Hadler. "Principles of Naval Architecture Series: Propulsion." The Society of Naval Architects and Marine Engineers (SNAME) (2010).

Kerwin, Justin E., and Chang-Sup Lee. Prediction of steady and unsteady marine propeller performance by numerical lifting-surface theory. No. Paper No. 8. SNAME Transactions, 1978.

Kinnas, Spyros A., Chan-Hoo Jeon, Jay Purohit, and Ye Tian. "Prediction of the unsteady cavitating performance of ducted propellers subject to an inclined inflow." In International symposium on marine propulsors SMP, vol. 13. 2013.

Kinnas, Spyros A., Yiran Su, Weikang Du, and Seungnam Kim. "A viscous/inviscid interactive method applied to ducted propellers with ducts of sharp or blunt trailing edge." In 31st Symposium on Naval Hydrodynamics Monterey, 2016

Kinnas, Spyros A., Wei Xu, Yi-Hsiang Yu, and Lei He. "Computational methods for the design and prediction of performance of tidal turbines." Journal of Offshore Mechanics and Arctic Engineering 134, no. 1 (2012): 011101.

Lee, Jin-Tae. A Potential Based Panel Method for the Analysis of Marine Propellers in Steady Flow. No. OE-87-13. Massachusetts Institute of Technology, Department of Ocean Engineering, 1987.

Lerbs, Hermann W. Moderately loaded propellers with a finite number of blades and an arbitrary distribution of circulation. Society of Naval Architects and Marine Engineers, Transactions, 1952.

Menéndez Arán, David Hernán. "Hydrodynamic optimization and design of marine current turbines and propellers." Master's Thesis, Ocean Engineering Group, The University of Texas at Austin (2013).

Menéndez Arán, David H., and Spyros A. Kinnas. "On Fully Aligned Lifting Line Model for Propellers: An Assessment of Betz condition." Journal of Ship Research 58, no. 3 (2014): 130-145.

Wrench Jr, J. W. The Calculation of Propeller Induction Factors AML Problem 69-54. No. DTMB-1116. DAVID TAYLOR MODEL BASIN WASHINGTON DC, 1957.

Xu, Wei. "Numerical techniques for the design and prediction of performance of marine turbines and propellers." Master's Thesis, Ocean Engineering Group, The University of Texas at Austin. (2010).

APPENDIX

Propeller case and duct case validation: spacing, convergence study and different initial conditions
For different cases, different spacing should be used, and the corresponding circulations are shown in Figure 23. In the shown figure, both the advance ratio and the thrust coefficient for the propeller case are 1.0; in the turbine case,

the tip speed ratio is 8. Other parameters are the same as in Table 1 and 2. In constant spacing with one ¼ inset and the half cosine spacing, more elements are concentrated where the gradient of the circulation is high. As shown in the figure, the half cosine or full cosine spacing agrees well with the constant spacing with one or two ¼ inset. In this paper, the propeller case has a duct but has no hub, so half cosine spacing is adopted. In the turbine case, the image models for both hub and duct are used, so constant spacing is applied.

(a) Propeller case　　　　　　　　　　　　**(b) Turbine case**
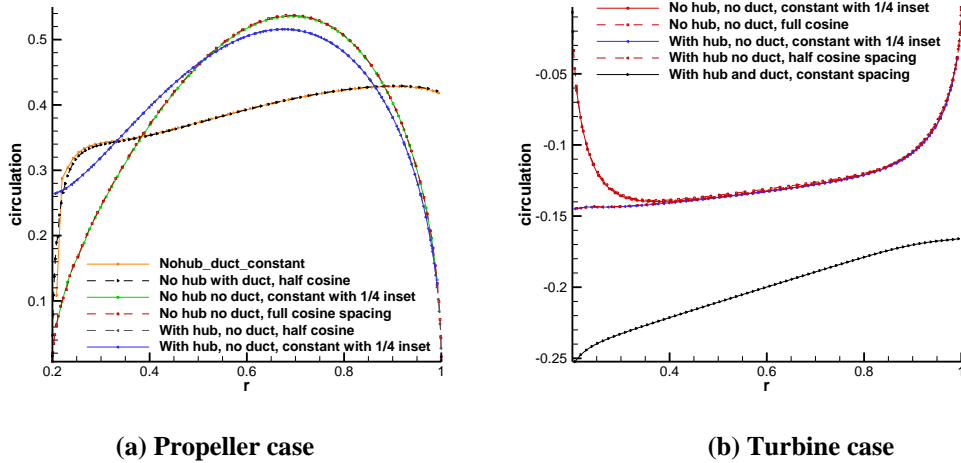
Figure 23 The circulation from different spacing

In this paper, 70 panels are used in the lifting line model for both the propeller case and the turbine case. As shown in Figure 24, smaller panel number is enough for both cases. However, since the lifting line code can run very fast, 70 panels are used throughout this paper for both propeller case and turbine case.

(a) Propeller case　　　　　　　　　　　　**(b) Turbine case**
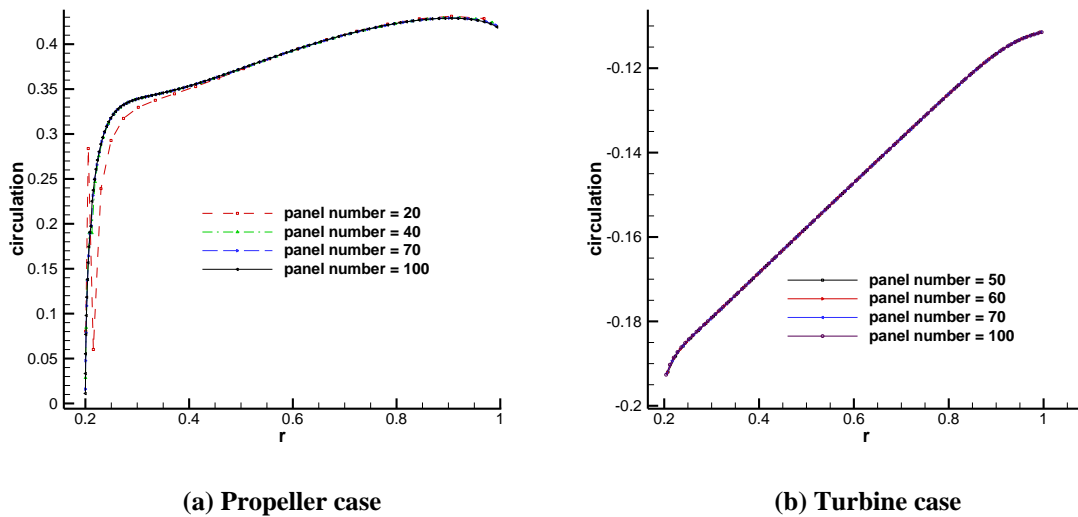
Figure 24 Convergence study for the lifting line model

To show that the RANS/lifting line model interaction method does not depend on the selection of initial values, three sets of initial inflow velocity and τ are selected in the propeller case as: U_{in}=1.0, τ = 1.0; U_{in}=0.8, τ = 1.2; U_{in}=1.2, τ = 0.8. After running LLOPT2NS, all the three cases converge to the same final solution, as shown in Figure 25.
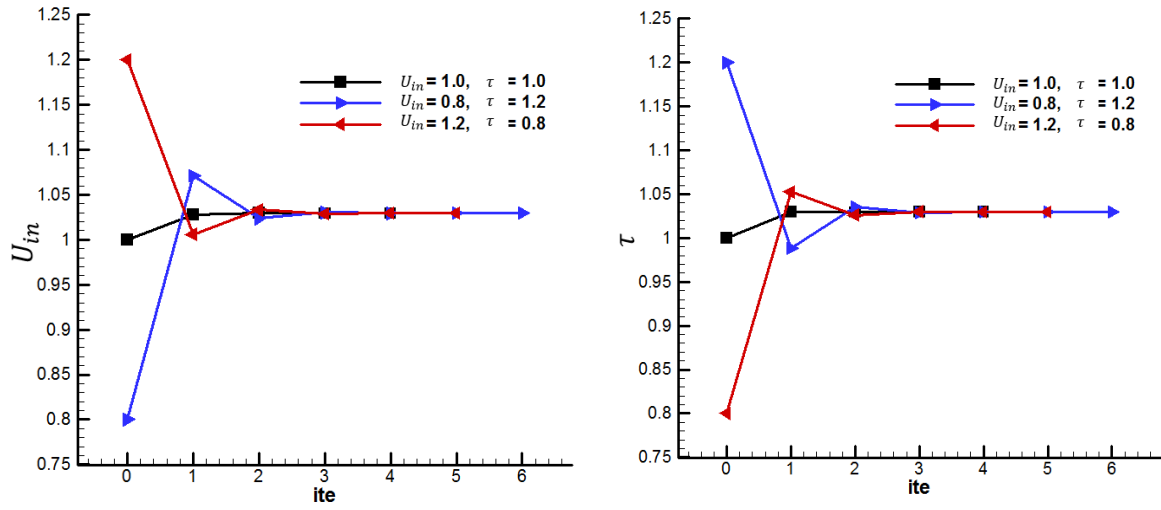
Figure 25 A propeller case by selecting different initial conditions